Department of Precision and Microsystems Engineering

Negative Stiffness in Compliant Shell Mechanisms

A.P.F. Broshuis

Report no	:	2019.013
Coach	:	Ir. J. Rommers
Professor	:	Prof. dr. ir. J.L. Herder
Specialisation	:	Mechatronic System Design
Type of report	:	Master Thesis
Date	:	11 April 2019

Negative stiffness in compliant shell mechanisms

To develop a passive stroke rehabilitation device

by

A.P.F. Broshuis

to obtain the degree of Master of Science
at the Delft University of Technology,
to be defended publicly on Friday April 26, 2019 at 10:00 AM.

Student number:	4223586	
Project duration:	February 15, 2018 – April 26, 2019	
Thesis committee:	Prof. dr. ir. J.L. Herder,	TU Delft
	Associate Prof. dr. M.Sc.Eng. C.J. Kim,	Bucknell University
	Ir. J. Rommers,	TU Delft
	Dr. ir. C. Ayas,	TU Delft

Delft University of Technology

Preface

This thesis is the final result of my master Precision and Microsystem Engineering at the faculty of Mechanical, Maritime and Material Engineering (3mE) at the Delft University of Technology. I am proud to graduate at one of the most technical disciplines here at Delft University of Technology.

I would like to thank Eveline, Joep and Werner for introducing me to this project. I would like to thank my supervisor Jelle for our extensive weekly meetings, reviewing my work and his advice. I would like to thank my professor Just Herder for his constructive feedback during our meetings in Delft, over Skype and even over dinner in Quebec City. I would like to thank Patrick Roest of TU Delft for his technical support with my experiment. Of course I would like to thank Charles for giving me the opportunity to come to Bucknell University and live in Lewisburg (PA) for 5 months. It was an amazing and enriching experience both as a student and as a person. I would like to thank you for our interesting and extensive meetings, your patience and guidance and for taking us on trips to the convention in Quebec City and the hospital in Washington D.C. I would like to thank Chad for his hospitality by letting me live at his place for 5 months and making my stay in Lewisburg very enjoyable. Finally I would like to thank my girlfriend, friends, parents and sister for their support throughout my study. Without you I would not have been able to do it.

A.P.F. Broshuis
Delft, April 2019

Contents

1 Introduction

Stroke rehabilitation therapy

In the United States 795.000 people experienced a stroke in 2018, this means one person every 40 seconds. Nearly 133.000 people were killed after having a stroke, which makes it ranked 5th among all causes of death in the USA. It also makes it the leading cause of serious long-term disability in the United States [2].

Rehabilitation is often done by movement therapy, which is based on neuroplasticity. Neuroplasticity is the ability of the brain to reorganize itself. Motor learning improves by doing exercises that are repetitive, goal-directed and intensive [11].

The focus of this thesis is on the rehabilitation of the upper-extremity. Patients that have suffered a stroke lost strength in one of their arms and are not able to lift it by themselves anymore. This is problematic for doing rehabilitation exercises. Different rehabilitation devices that balance the gravity of the arm are currently available. Most of them are active devices that must be used in a clinical environment under the supervision of a doctor or a physiotherapist. Passive devices that can be used at home are available, however they are not wearable and often require large constructions. Therefore a device that is wearable and can be singly used by the patient at home is what is missing. The patient should be able to use the device without any assistance and the donning and doffing must be possible individually.

A compliant shell mechanism could overcome the shortcomings of the current available devices. By the use of monolithic shell mechanisms a simple to use device can be designed, which can be made wearable. It would make it easier for stroke rehabilitation patients to do rehabilitation exercises at home.

Static balancing

To balance the gravity of the arm it has to be statically balanced at every position over a range of motion that is needed for rehabilitation exercises. The flexion and extension of the elbow during the lifting of the arm changes the needed moment around the shoulder for the static balancing of the arm. This creates a more complex problem. To avoid the influence of the lower-arm the elbow is assumed as a rigid connection and the lower-arm is assumed as being stretched out in all positions.

Force equilibrium over the whole trajectory is needed for static balancing, meaning that the gravitational force of the arm has to be compensated for every position. From an energy perspective the static balancing of the arm means that the potential energy has to be constant for every position.

The attachment of the compliant shell mechanism to the patient determines what behavior it needs to have for balancing the gravity of the arm. For simplicity of the device there is chosen for a fixed-fixed attachment. Static balancing requires negative stiffness behavior of the shell over a large rotational range of motion.

Thesis outline

The body of this thesis consists of two chapters based on the needed negative stiffness to statically balance the arm if the shell mechanism has a fixed-fixed attachment to the patient. One of these chapters is written as an independent paper.

In chapter 2 it is elaborated how negative stiffness is used for stroke rehabilitation therapy. The problem statement and the needed negative stiffness is described for a fixed-fixed attachment of the shell to the patient.

Chapter 3 is written as an independent paper and is the key contribution of this master thesis. The paper describes how a longer range of negative stiffness over a rotational range of motion can be obtained in compliant shell mechanisms.

The thesis ends with further recommendations and the conclusion. The appendices are attached at the end and provide more information about stroke rehabilitation therapy and about the potential of curved corrugated shells for tune-able negative stiffness.

2

Negative stiffness for stroke rehabilitation therapy

The human arm can be divided into two parts, the upper-arm and the lower-arm. The upper-arm is connected to the shoulder and can be modelled as a rigid beam connected to a pivot, the shoulder, at one end. At the other end it has a joint, the elbow, which connects it to another beam, the lower-arm. Due to the elbow the upper- and lower-arm can rotate independently. When the lower-arm is rotated around the elbow the position of the centre of gravity of the lower-arm changes relative to the upper-arm. To avoid this influence of the lower-arm on the balancing of the arm, the elbow is assumed as a rigid connection that connects the upper- and lower-arm. The lower-arm is not rotating around the elbow and maintains in the same position relative to the upper-arm.
The movements of the upper-arm are shown in fig.2.1. The upper-arm is needed for various activities of daily

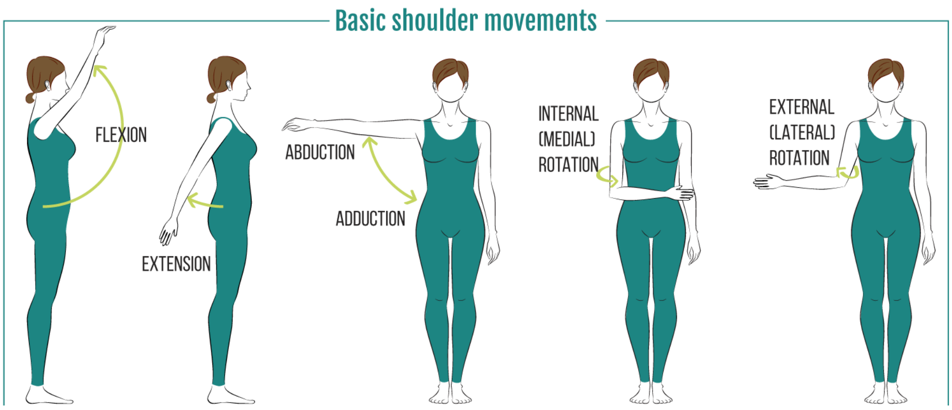

Figure 2.1: Basic movements of the shoulder [6]

living (ADL). For the majority the abduction, adduction, flexion and extension are necessary for performing these ADL [11]. Therefore the focus is on balancing the arm during these movements. For most ADL the necessary range of motion is between 0° and 90° [4]. At 0° the arm is vertical next to the body and at 90° the arm is lifted to a horizontal position.
The stroke rehabilitation device has to be attached at the shoulder and at the upper-arm before the elbow. Attachment of the device to the lower-arm will induce the flexion of the elbow, which is undesired behavior. The upper-arm is modelled as a hanging pendulum with a range of motion from 0° to 90° rotation. The lower-arm is modelled as a point mass at the end. Fig. 2.2 shows the hanging pendulum with the attached point mass for the lower-arm.

The pendulum has to be balanced over the full range of motion. The lifting of the arm changes the moment-arm of the gravitational force to the shoulder. The moment around the shoulder induced by the weight of the arm during the rotation and the needed moment to statically balance the arm are shown in fig. 2.3. A moment of the same magnitude in the opposite direction is needed for the static balancing of the arm.

Since the mechanism will have a fixed-fixed attachment to the arm it can be modelled as a torsion spring. This means that the desired moment is determined by the equation for rotational stiffness:

$$M = -k * \theta \tag{2.1}$$

The negative sign in the equation shows that when the arm is rotated along the direction of θ, the spring is elongated and therefore produces an increasing moment in the opposite direction. The initiated moment would be in the counter clockwise direction of fig. 2.2 However, if the arm is lifted the moment has to be increasing in the same direction as the rotation. Therefore, a negative stiffness is necessary. When θ is increasing, the moment has to be increasing as well.

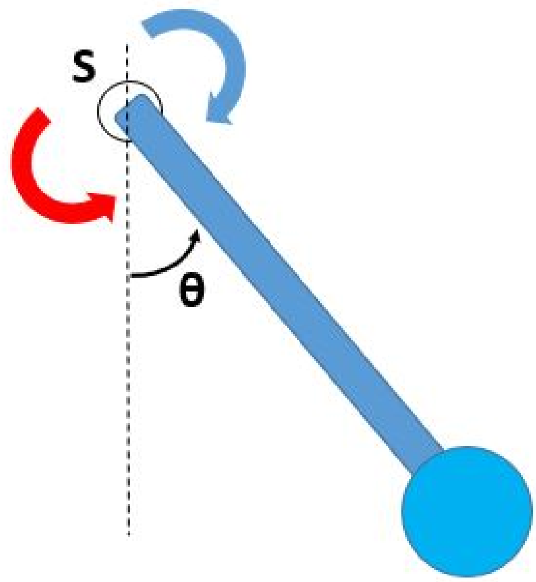

Figure 2.2: The upper-arm modelled as a hanging pendulum with the lower-arm as a point mass. The *S* indicates the shoulder. The blue arrow indicates the direction of the moment due to the weight of the arm. The red arrow indicates the direction of the moment needed for balancing the arm.

To obtain this desired moment a constant force normal to the arm in combination with a negative stiffness is needed. The constant force creates a constant moment around the shoulder. The magnitude of the moment needs to be able to balance the maximum moment due to the weight of the arm. This maximum arises when the arm is in horizontal position ($\theta = 90°$). In fig. 2.4 the desired moment and the moment due to the constant force normal to the arm are shown. At the vertical downward position of the arm ($\theta = 0°$) zero moment is required. To balance the moment due to the constant force the stiffness of the shell has to be at its maximum when the arm is vertically downward. During the upward rotation of the arm the stiffness has to decrease and be close to zero when the arm is held horizontally. Accordingly a decreasing negative stiffness is necessary for balancing the arm as shown in fig. 2.5.

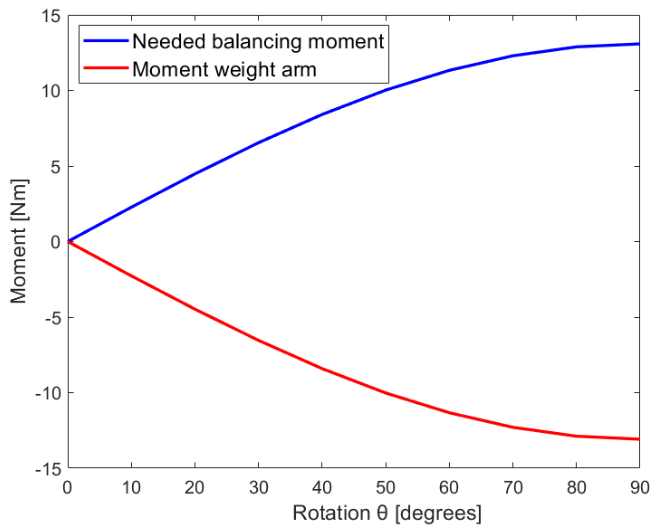

Figure 2.3: The desired moment and the moment due to the weight of the arm over the range of motion of the arm.

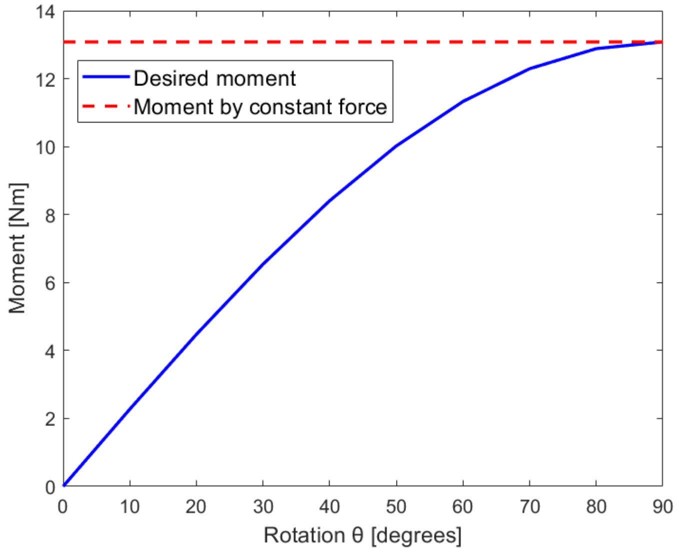

Figure 2.4: The moment induced by the constant force that acts normal to the arm and the moment due to the weight of the arm that has to be balanced.

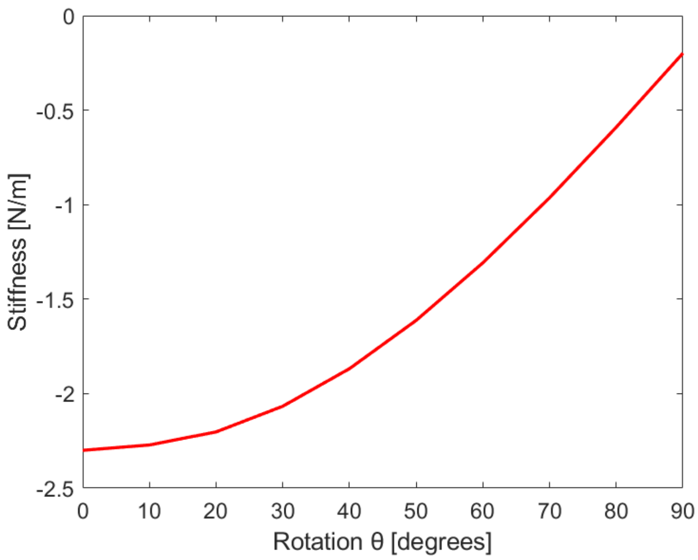

Figure 2.5: Desired negative stiffness of the compliant shell mechanism. The negative stiffness has to be decreasing over the range of motion.

3

Paper: Negative Stiffness in Compliant Shell Mechanisms

Negative Stiffness in Compliant Shell Mechanisms

Ab P.F. Broshuis[1], Charles J. Kim[2], Jelle Rommers[1], Just L. Herder[1]

[1] *Department of Precision and Microsystems Engineering, Delft University of Technology*
[2] *Department of Mechanical Engineering, Bucknell University*

Abstract

Compliant shell mechanisms are thin-walled structures that use their elastic deformation to transfer or transmit force, motion or energy. Tape springs are thin-walled beams with a curved cross section, wherein sudden negative stiffness for a short range of motion arises during buckling. The short range of the negative stiffness limits the use for static balancing over a longer range of motion. In this paper, an analysis is presented on how the range of the negative stiffness can be increased by changing the geometry. The addition of longitudinal curvature to the tape spring results in a more gradual negative stiffness for a longer range of motion. An experiment shows the change in behavior during the instability and confirms the elongation of the range of negative stiffness.

1 Introduction

Compliant shell mechanisms are being investigated more and more. Leemans [1] recently described them as: "Compliant shell mechanisms utilize spatially curved thin-walled structures to transfer or transmit force, motion or energy through elastic deformation." Due to their spatial geometry they are useful as building blocks for spatial mechanism design. Radaelli and Herder [2] used a computational method to design a compliant shell mechanism gravity balancer. Nijssen [3] created a library of different shell building blocks and described them by their compliance vectors. Describing the shells analytically is necessary for designing mechanisms.

The research to the use of elastic structural instabilities for applications increased over the last decade. Herein an increasing interest for buckling, for centuries seen as a disadvantage in design, arised and it is more and more identified as a favourable behavior. Hu and Burugeno [4] stated a long review of the recent advances in buckling-induced smart applications mentioning energy- and motion-based applications.

Hoetmer [5] characterized three negative stiffness compliant 2D building blocks by the use of compressed plate springs used to design a statically balanced compliant mechanism. The negative stiffness was added as a balancing segment to cancel the positive stiffness.

The negative stiffness in spatial compliant shell mechanisms has been investigated for the tape-spring. Seffen [6] describes tape springs as thin-walled beams with a curved cross-section that can be elastically deformed to yield a flexible region of high curvature. Seffen et al. [7] investigated the folding and deployment of curved tape springs. Hereby the end effect differences between curved and straight tape springs were defined. The constant moment after the snap-through of the tape spring was investigated for deployable structures in space.

Seffen [6] used the instability to initiate the deployment of structures, however the negative stiffness behavior during the instability is not investigated. The abrupt and short range of negative stiffness in a tape spring is not useful for a longer range of rotation. A clear advantage of the elongation of the range of negative stiffness behavior is that it contributes to the static balancing of rotational mechanisms.

In this paper it is shown how the range of negative rotational stiffness in compliant shell mechanisms can be elongated. This is a new way of using the instability that occurs during the rotation of compliant shell mechanisms with transverse curvature, e.g. tape springs.

The paper is structured as follows. Section 2 describes that a sudden negative stiffness arises during the buckling of a tape spring and shows that the addition of longitudinal curvature elongates the range of the negative stiffness. Section 3.1 defines the stress and strain energy behavior and the deformation of the cross section in the tape spring before the instability and in section 3.2 this is done for the hyperbolic-parabolic. Hereafter, section 3.3 declares the differences between both shells during the instability. The elongated range of negative stiffness is validated by an experiment in section 4. The results of the experiment and the contribution of this paper are discussed in section 5. A brief summary and a general conclusion is given in section 6.

2 Background

The objective of this paper is to elongate the range of the negative stiffness that occurs in the tape spring during the structural instability. Fig. 1a shows the investigated tape spring. The top and bottom are both rigid planes, the bottom is fixed to the ground and it has a thickness of $2mm$. The red lines indicate the transverse curvature and the longitudinal curvature is zero. The rotation α is applied at the middle of the top around the y-axis against the transverse curvature. The following equations are used to create the curvatures of the shell:

$$X_{transverse} = aY^2 \tag{1}$$

$$X_{longitudinal} = bZ^2 \tag{2}$$

Where a is kept constant at a value of 40, resulting in a constant transverse curvature, and b varies to add longitudinal curvature.

In fig. 2 it can be seen that buckling occurs for a tape spring ($b = 0$) after a moment is reached that is greater than a certain critical load. There is a sudden drop of the moment that is needed to rotate the curve. The derivative of the moment-rotation plot results in the stiffness and it is negative during the instability as can be seen in fig. 2.

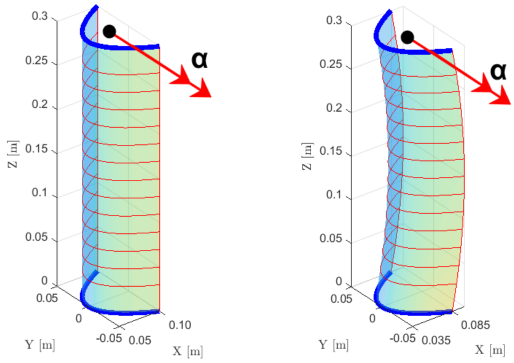

(a) (b)

Figure 1: (a) Dimensions of the tape spring. (b) Dimensions of the hyperbolic-parabolic. The transverse curvature is in the XY-plane and the longitudinal curvature in the ZX-plane. The red arrows indicate the direction of rotation α with the black dot as point of application. The blue lines indicate the rigid ends of both shells.

The integral of the moment-rotation curve is the energy-rotation curve of the shell, which will be the strain energy due to the bending. For the tape spring this will result in a positive increasing energy curve until the instability. At the instability the energy will remain constant and have a gradient of zero, the result is a sudden negative stiffness behavior. After the instability it will be barely increasing since the tape spring has barely any stiffness left.

To make the negative stiffness useful for a longer range of motion it has to happen more gradually and over a longer part of the rotation. A sudden decrease in total strain energy during the instability, wherein the gradient becomes zero or negative resulting in a sudden negative stiffness is not desired. The gradient of the strain energy rotation plot has to be positive decreasing instead during the instability. This means that during the instability less energy has to be used for the next degree of rotation α than the degree of rotation before. However, the total strain energy is not decreasing or constant if the shell is rotated during the instability.

Increasing b in equation 2 adds longitudinal curvature to the shell. Adding longitudinal curvature results in a more gradual negative stiffness. This result is found in an internal developed software based on IGA at Delft University of Technology. The tape spring obtains a negative Gaussian curvature and becomes a hyperbolic-parabolic. Fig. 2 shows that for a hyperbolic-parabolic with a small longitudinal curvature the sudden negative stiffness maintains. However, by adding more longitudinal curvature the negative stiffness becomes more gradual.

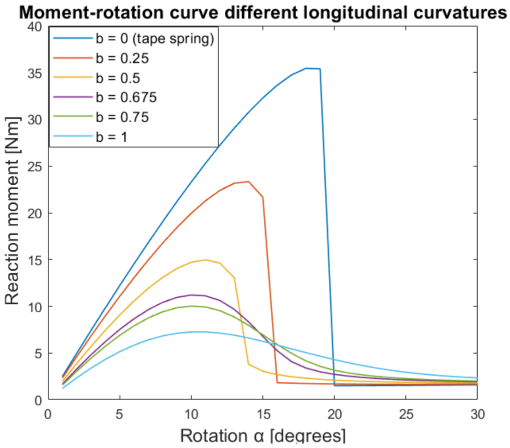

Figure 2: Moment-rotation curves for different longitudinal curvatures. The tape spring has zero longitudinal curvature ($b = 0$). The negative stiffness becomes more gradual for increasing b.

3 Method

An analysis is made on both the tape spring and the hyperbolic-parabolic to determine why the negative stiffness becomes more gradual. In fig. 1b the dimensions of the tape spring and hyperbolic-parabolic are shown. At first the analysis on the straight tape spring is done. The stress, deformation and strain energy before the instability are investigated for an imposed rotation α. Thereafter it is investigated what changes in the tape spring when longitudinal curvature is added and what the results of this are on the stress, deformation and strain energy before, during and after the instability for an imposed rotation α.

3.1 Tape spring analysis

An image of the tape spring with its dimension system is shown in fig. 1a and its cross section is shown in fig. 3. The ends of the cross section at the maximum and minimum of the y-axis are referred to as points S and the part at the minimum of the x-axis is referred to as point M.

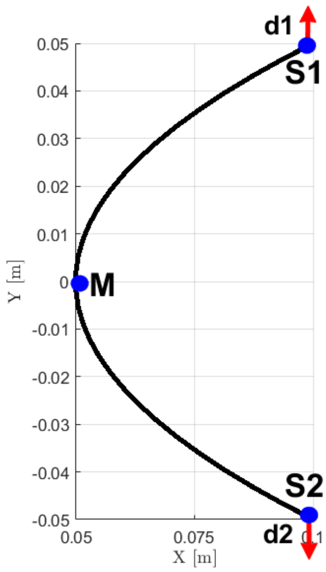

Figure 3: Dimensions of the cross sections of the tape spring and hyperbolic-parabolic. Point M lies halfway the height of the shell at the side referred to as the *middle*. Point $S1$ and $S2$ lie halfway the height of the shell at the side referred to as the *sides*. $d1$ is the displacement of $S1$ in the Y-direction and $d2$ the displacement of $S2$ in the y-direction. More flattening means a larger displacement $d1$ in the positive y-direction and a larger displacement $d2$ in the negative y-direction.

3.1.1 Deformation of the cross section

The shell is assumed as being quasi-static during the rotation, meaning that for every applied rotation α the shell is in equilibrium. Equilibrium dictates that every deformed configuration is at a state of minimum potential energy. Brazier [8] described that if one dimension of the cross section is small compared to others, large displacements over the cross section may occur. It is inaccurate to assume the stress as a linear function and higher order terms cannot be neglected. The thickness in shells is small compared to the other dimensions and therefore Braziers effect [8] applies to them. The displacements of the cross section are directed in a way that the forces in the shell initiating the displacements do no work. It is therefore stated that the displacements due to the flattening have the result that the shell is in a lower state of potential energy, i.e. the strain energy of the shell is at a minimum.

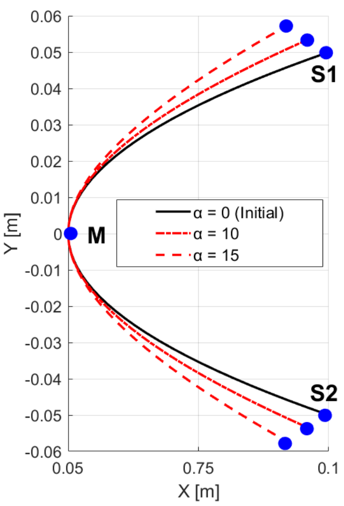

Figure 4: Deformation of the cross section of the tape spring for different rotations α. $S1$ moves in the positive Y-direction and $S2$ in the negative Y-direction.

The cross section of the tape spring deforms when a rotation α is applied. The cross section flattens and deforms to a shape with less transverse curvature. The flattening is measured by the displacement of points $S1$ and $S2$ in the Y-direction, where $S1$ moves in the positive and $S2$ moves in the negative Y-direction. In fig. 4 the deformation of the cross section of the tape spring is shown for different rotations α.

An analysis on the strain energy in the tape spring is made in ANSYS to verify if this occurs as a result of the shell obtaining a state of lower potential energy. No deformation occurs in the cross section if the non-linearities for large deflections are switched off to neglect the effect of higher order terms. The total strain energy with and without the effect of the deformation of the cross section is compared and is shown in fig. 5a. It can be seen that the strain energy in the shell is lower when the cross section flattens. Therefore it is stated that the deformation of the cross section occurs since a state of lower potential energy is achieved.

3.1.2 Stress distribution in the shell

The strain energy decreases in the shell due to the flattening of the cross section. Strain energy is calculated by: $U = \frac{1}{2}\frac{V}{E}\sigma^2$, and therefore the integration of the stresses in the shell has to decrease as well. To create an image of what stresses are decreased by the flattening a comparison has to be made between the stress analysis of the case wherein the flattening is and is not considered.

The expected stress distribution of the shell can be estimated if flattening is ignored. Stresses in the z-direction will arise due to the bending of the shell. A neutral axis, where the stress is zero, will arise with compression at the side of point M and tension at the side of points S. The stress distribution will be calculated by the equation $\sigma = \frac{My}{I}$. Herein is y the distance to the neutral axis, meaning that the stress is distributed linear and increases at positions further away from the neutral axis.

In ANSYS an analysis is done to obtain the stress distribution in the tape spring when the flattening is ignored. As expected it is a linear line crossing the line of zero stress at its neutral axis. A second analysis is done wherein the flattening is not ignored. A comparison is made between the stresses for both

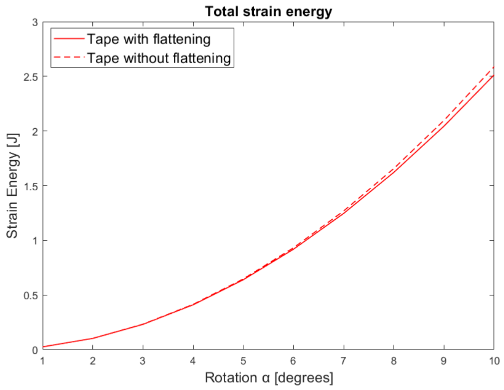

(a) Total strain energy during the rotation

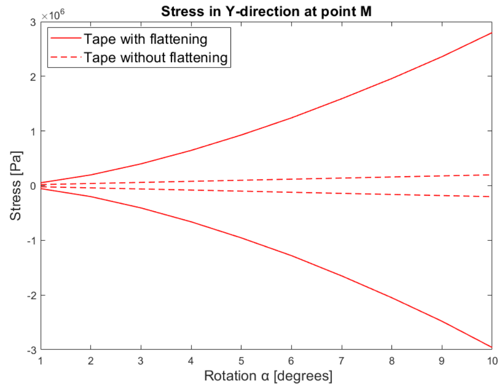

(b) Y-direction stress at point M during the rotation

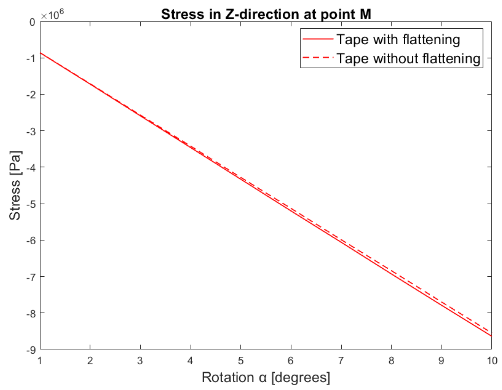

(c) Z-direction stress at M during the rotation

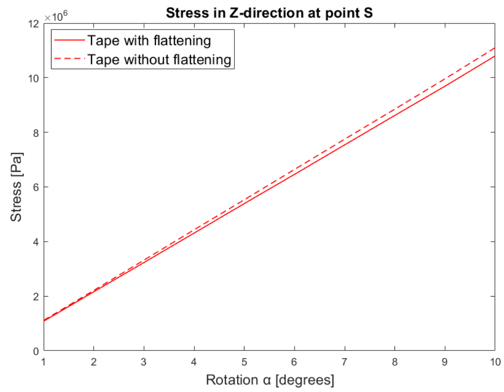

(d) Z-direction stress at point S during the rotation

Figure 5: Effects of the flattening of the tape spring before the instability.

analysis. The stresses with the most relevant changes between the two analysis are displayed in fig. 5. The positions and directions are clarified in fig. 1a and fig. 3. It can be stated that the tension stress in the z-direction at points S decreases due to the flattening of the cross section and the compression stress in the z-direction at point M barely changes. Stresses in the y-direction initiate at point M if the shell is flattened. This is a logical result since those stresses arise due to the deformation of the cross section.

3.1.3 Effect on the strain energy

The decreasing stresses at points S in the z-direction indicate a decrease of the strain energy density at the sides of the shell and a decrease in the strain energy. The increasing stress in the y-direction at point M indicates an increase in the stain energy density at the middle of the shell, which means an increase in strain energy at the middle. Due to the flattening of the cross section a state of lower total strain energy is achieved. Therefore the flattening must result in a greater total decrease than total increase in strain energy.

To clarify this the flattening is now seen as a behaviour that is separate from the bending of the shell. The shell is kept at a constant rotation α. If the cross section would not have been deformed no flattening would have occurred and there would have been a higher total strain energy in the shell. The total strain energy would be higher due to the higher strain energy density at the sides, despite the lower strain energy density at the middle due to a smaller deformation of the cross section. If the cross section would have been flattened further than the equilibrium state the opposite would happen. Due to the larger deformation of the cross section the strain energy density at the middle would be increased. The strain energy density at the sides would decrease due to the extra flattening of the cross section. The total strain energy would however increase since the strain energy at the middle would become more dominant. In fig. 6 it is visualized that for less flattening the shell will have a higher total strain energy due to the energy at the sides and for more flattening it will have a higher total strain energy due to the strain energy at the middle. For every rotation α of the shell the cross section flattens until the point where the total strain energy would start increasing. This indicates that the total strain energy is at a minimum.

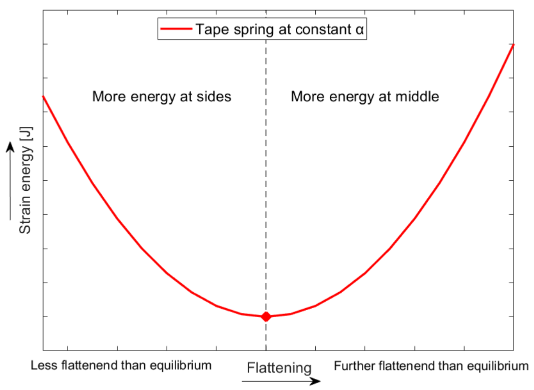

Figure 6: Effect of the flattening on the strain energy in the tape spring for a constant rotation α. The red dot indicates the equilibrium, where the strain energy is at its minimum.

3.2 Analysis hyperbolic-parabolic

The longer range of negative stiffness is obtained if longitudinal curvature is added to the tape spring, which changes it to a hyperbolic-parabolic. The longitudinal curvature changes the stress distribution of the shell and therefore the strain energy density through the shell. It will now be elaborated how the stress distribution changes when longitudinal curvature is added to the shell.

3.2.1 Influence longitudinal curvature

For the tape spring the neutral axis passes through the centroid of the cross-section since a pure bending moment is applied and no axial forces are acting on the cross-section. The neutral axis coincides with the centroidal axis. However, the addition of longitudinal curvature changes the position of the neutral axis. By the use of the Winkler-Bach equation [9] the change in stress distribution can be estimated. For a curved shape the strain is calculated as follows:

$$\epsilon = \frac{\delta l}{l} = \frac{(r - r_n)}{r}\frac{d\phi}{\phi} \tag{3}$$

Where r_n is the radius from the centre of curvature to the neutral axis and r is the distance from a position of the shell to the centre of curvature. For the stress-strain equation this results in:

$$\sigma = \epsilon E = E\frac{(r - r_n)}{r}\frac{d\phi}{\phi} \tag{4}$$

Since pure bending is applied to the shell no external forces are acting:

$$\int \sigma dA = E\frac{d\phi}{\phi}\int \frac{(r - r_n)}{r} dA = 0 \tag{5}$$

By simplifying equation 5 the equation for the determination of the position of the neutral axis is obtained. The cross section is assumed as being homogeneous, which makes E constant.

$$r_n \int \frac{E}{r} dA - \int E dA = 0 \tag{6}$$

$$r_n = \frac{A}{\int \frac{dA}{r}} \tag{7}$$

Substituting the radius from the centre of longitudinal curvature of the shell to the centroid of the shell for r in equation 7 shows that the neutral and centroidal axis are not equal to each other anymore due to the addition of the longitudinal curvature. This means that they do not coincide anymore and that there is a shift in the location of the neutral axis. By balancing the external applied moment against the internal resisting moment the resulting stress is derived. The resisting moment is the integral over the section of the moment arm ($y = r_n - r$) multiplied by the force ($dF = \sigma dA$). Together with equation 5 this leads to the moment equation:

$$M = E\frac{d\phi}{\phi}(-r_n\int dA + \int rdA) \tag{8}$$

$$M = E\frac{d\phi}{\phi}(r_c - r_n)A \tag{9}$$

Eventually by using equation 4 the following equation for the stress distribution can be stated: (4)

$$\sigma = \frac{M(r - r_n)}{Ar(r_c - r_n)} \tag{10}$$

Equation 10 makes it clear that the stress distribution becomes hyperbolic instead of linear when longitudinal curvature is added.

3.2.2 Stress distribution

If longitudinal curvature is added to the tape spring the neutral axis shifts towards the centre of the longitudinal curvature and the stress distribution becomes hyperbolic instead of linear. Fig. 7 shows the stress distribution over the shells for the same applied moment and if for both the tape spring and the hyperbolic-parabolic the flattening of the cross section is ignored. The change in stress distribution results in higher tension stress at the sides (points S) and higher compression stress at the middle (point M) in the z-direction.

It can be seen that due to the hyperbolic stress profile the tension stress becomes less decreasing from the sides (points S) towards the neutral axis if longitudinal curvature is added. For the same volume the strain energy density at the sides increases due to the addition of longitudinal curvature. This is an important result, since for the tape spring the strain energy is released at the sides during the flattening of the cross section.

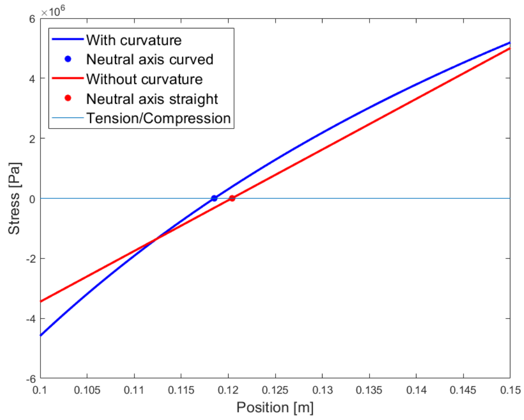

Figure 7: Difference in stress distribution if longitudinal curvature is added. Point M is at the minimum and points S are at the maximum of the x-axis.

3.2.3 Effect on the deformation of the cross section

The addition of longitudinal curvature increases the strain energy density at the sides. The result is that for the hyperbolic-parabolic more energy is released at the sides compared to the tape spring if the cross section flattens.

To clarify this the flattening is treated again as a behavior that is separate from the bending of the shell. Rotation α is again kept constant. When the cross section of the shell flattens the energy at the sides decreases and the energy at the middle increases. The strain energy density at the sides is higher for the hyperbolic-parabolic than for the tape spring if the shells are kept at a constant rotation α and if flattening is not accounted for. Therefore the flattening of the cross section results in a higher decrease of energy at the sides for the hyperbolic-parabolic compared to the tape spring. For the hyperbolic-parabolic the total strain energy decreases

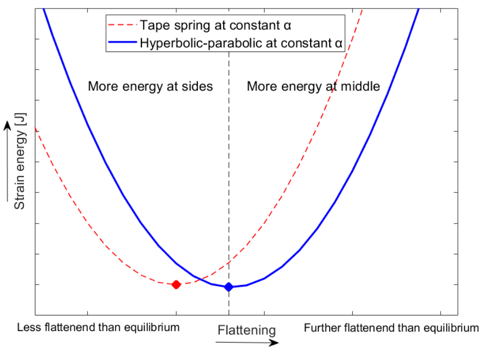

Figure 8: Effect of the flattening on the strain energy in the hyperbolic-parabolic for a constant rotation α. The blue dot indicates the equilibrium, where the strain energy is at its minimum. The equilibrium is reached at a larger deformation of the cross section for the hyperbolic-parabolic compared to the tape spring. Since more energy is released at the sides it takes more deformation before the energy at the middle starts increasing the total energy.

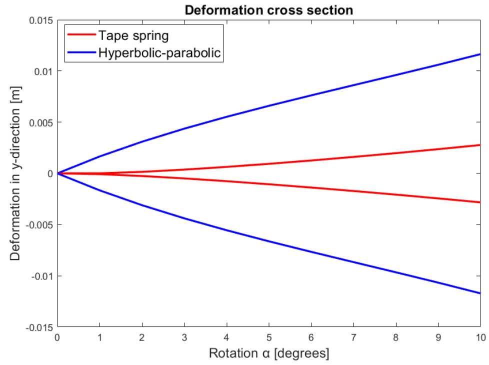

Figure 9: The deformation of the cross section for both shells before the instability. The deformation is measured by the displacement of the points S in the y-direction for both shells. The lines in the positive y-direction are the displacement of $S1$, in the negative y-direction the displacement of $S2$.

for a larger deformation of the cross section despite the increase in strain energy at the middle. The point where the flattening starts increasing the total strain energy occurs at a larger deformation of the cross section. This is illustrated in fig. 8.

The hyperbolic-parabolic achieves a state of minimum potential energy by a greater deformation of the cross section compared to the tape spring. The result is that for the same rotation α of both shells, the cross section of the hyperbolic-parabolic deforms more than the cross section of the tape spring. The difference in the deformation of the cross section between the two shells is shown in fig. 9. The lines in the positive y-direction are the displacement of point $S1$ for both shells, the lines in the negative y-direction are the displacement of point $S2$.

An analysis on the stresses is done in ANSYS to validate that the higher decrease in strain energy density at the sides results in more flattening for the hyperbolic-parabolic during the rotation. The difference between the stresses in the hyperbolic-parabolic with and without flattening is analyzed and compared to the stresses in the tape spring. In fig. 10d it is clear that for a rotation α more tension stress is released at point S for the hyperbolic-parabolic than for the tape spring due to the flattening of the cross section. There is a higher decrease in the compression stress at point M in the z-direction for the hyperbolic-parabolic and a higher increase in stress in the y-direction at point M due to the flattening (Fig. 10).

The higher decrease in stress at point S for the hyperbolic-parabolic with flattening compared to the hyperbolic-parabolic without flattening indicates the higher decrease of strain energy density at the sides due to the flattening. The release of energy at the sides is higher for the hyperbolic-parabolic than for the tape spring. The larger increase in stress in the y-direction at point M for the hyperbolic-parabolic is a reaction on the greater deformation of the cross section of the hyperbolic-parabolic.

For the hyperbolic-parabolic more energy is released at the sides due to the deformation of the cross section compared to the tape spring. Because of this higher release of energy at the sides, the increase in energy at the middle can be larger for the hyperbolic-parabolic than for the tape spring. The

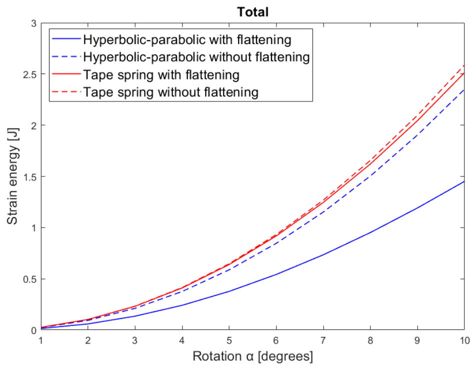

(a) Total strain energy during the rotation

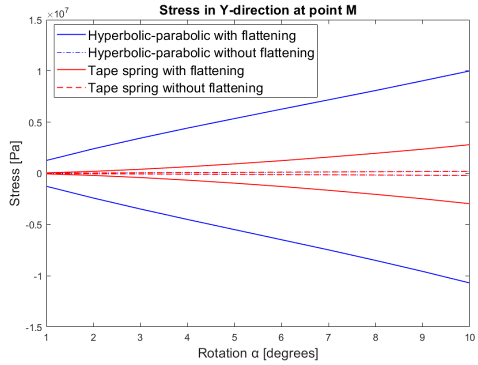

(b) Y-direction stress at middle during rotation

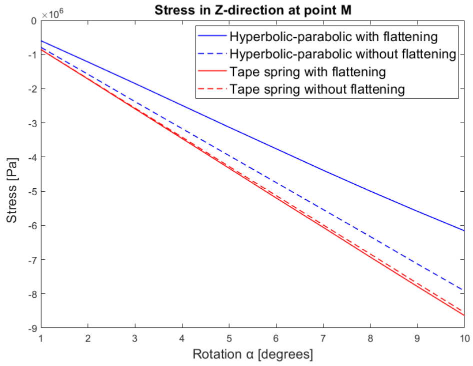

(c) Z-direction stress at middle during rotation

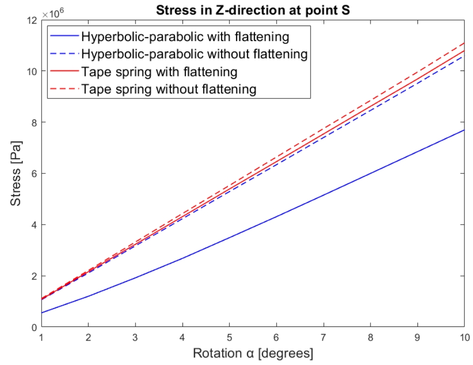

(d) Z-direction stress at sides during rotation

Figure 10: Difference in effects of the flattening on the tape spring and the hyperbolic-parabolic before the instability.

balance of the energy decrease at the sides and the increase at the middle results in a larger deformation of the cross section. It takes more deformation until the increase in energy at the middle is too large and does not result in a lower state of potential energy but in an increase in potential energy. Therefore, the cross section of the hyperbolic-parabolic has a larger deformation than the tape spring per angle of rotation α. More flattening results therefore in a lower total strain energy. From fig. 10a it is clear that the flattening in the hyperbolic-parabolic leads to a lower state of potential energy and that due to the flattening more energy is released compared to the tape spring .

Adding longitudinal curvature to the tape spring results in more flattening per angle of rotation and changes the energy distribution through the shell.

3.3 Behavior during the instability

In this section it is discussed what happens to both the tape spring and the hyperbolic-parabolic during the instability in terms of the flattening of the cross section, the strain energy and the stress distribution. By comparing both shells it is stated why the tape spring shows a sudden negative stiffness behavior and the hyperbolic-parabolic a more gradual negative stiffness behavior.

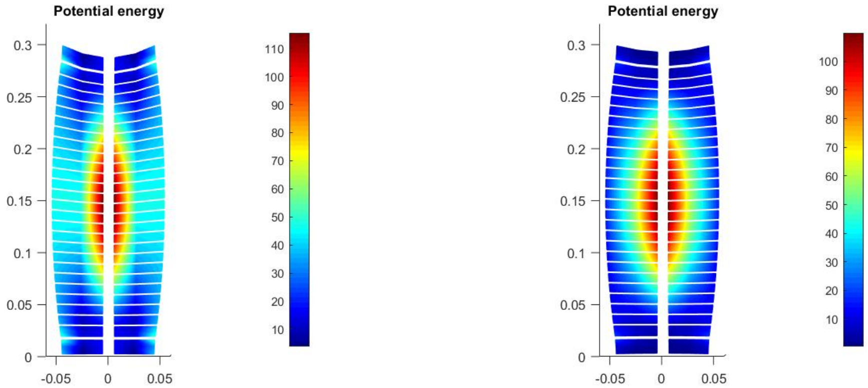

(a) Potential energy tape spring (b) Potential energy hyperbolic-parabolic

Figure 11: Energy distribution of both shells right before the instability occurs. For the tape spring there is still energy at the sides, for the hyperbolic-parabolic there is not.

In general a structure becomes unstable when a critical buckling load is reached. During this instability a state of lower potential energy is achieved mostly due to large deformations.

The longitudinal curvature in the hyperbolic-parabolic results in a different distribution of the stress through the shell compared to the tape spring. The strain energy density develops differently during the bending of the shell due to the added longitudinal curvature. For both shells the strain energy decreases at the sides and increases at the middle during the instability. The result is a transition of the energy from the sides to the middle. The behavior during the instability differs for the tape spring and hyperbolic-parabolic, due to the different development in strain energy density before the instability. Fig. 11 shows the distribution of the strain energy of both shells right before the instability. Where for the tape spring a significant part of the strain energy is still at the sides right before the instability, this energy is already released for the hyperbolic-parabolic. For the hyperbolic-parabolic a large part of the transition of the energy from the sides to the middle already occurred before the instability.

During the instability the cross sections of the tape spring and the hyperbolic-parabolic deform. Fig. 12c shows the changing deformation during the bending of both shells. The cross section of the hyperbolic-parabolic deforms more per degree of rotation α and has a more gradual increase during the instability. The tape spring has a sudden increase in deformation during the instability.

The total strain energy in both shells is shown in fig12d. For the tape spring the total strain energy suddenly decreases during the instability. The result is a sudden negative stiffness. For the hyperbolic-parabolic there is no decrease in total energy during the instability. However, the gradient of the energy changes from being positive increasing to positive decreasing. Rotating the shell a degree α further takes less energy than the rotation of the degree before that. The gradual change in total energy during the instability results in a more gradual negative stiffness over a longer range.

An analysis in ANSYS is done to investigate the changing stress distribution and strain energy density of both shells during the instability. Fig. 12a shows the stress in the z-direction at points S and fig. 12b the stress in the y-direction at point M during the bending of the shells.

For the tape spring the stress at the sides, indicated by points S, increases before the instability and at

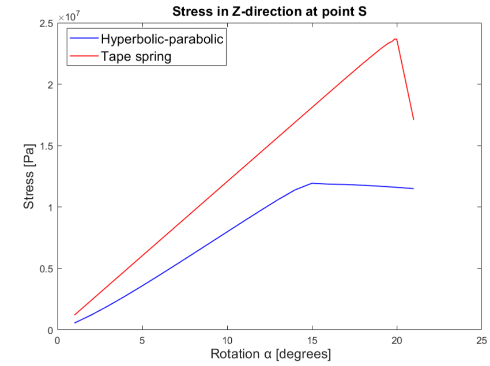

(a) Z-direction stress at sides during the instability

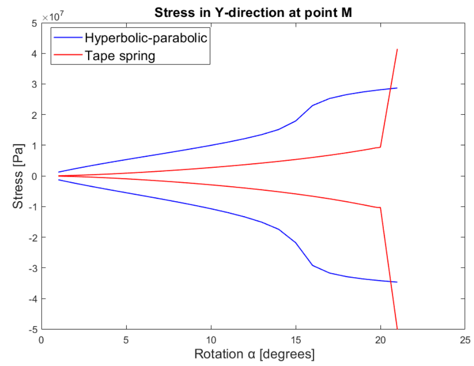

(b) Y-direction stress at middle during the instability

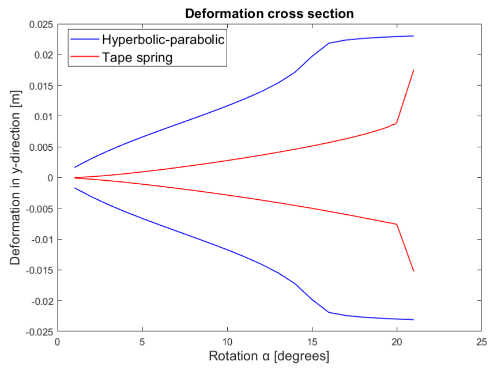

(c) Deformation cross section during the instability

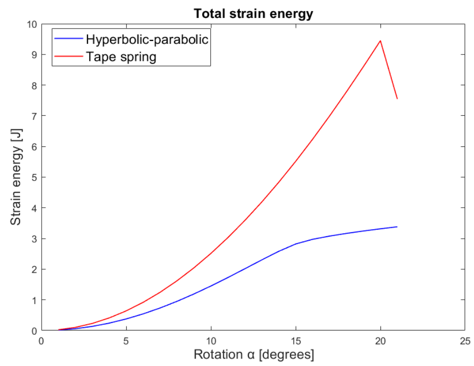

(d) Total strain energy during the instability

Figure 12: Behavior of both shells if bent past their instability. The instability of the tape spring occurs at 20°; The instability of the hyperbolic-parabolic occurs at 14°.

the instability suddenly decreases. The strain energy density at the sides decreases and indicates a release of strain energy at the sides. The stress at the middle, indicated by point M, suddenly increases due to the sudden deformation of the cross section. The strain energy density increases at the middle, which implies an increase in strain energy at the middle. The sudden decrease in strain energy at the sides is greater than the sudden increase in strain energy at the middle. The result is a decrease in total strain energy in the shell (fig. 12d).

For the hyperbolic-parabolic the stress at the sides, indicated by points S, decreases at the instability and the stress at the middle, indicated by point M, increases due to the deformation of the cross section. However, the decrease in stress at the sides is lower and less abrupt compared to the tape spring, which indicates a more gradual decrease in strain energy at the sides. At the middle the stress increases more gradual, which indicates a more gradual increase in strain energy at the middle. The total strain energy in the shell does not decrease due to the relative lower decrease in energy at the sides. However, the gradient of the total strain energy changes from positive increasing to positive decreasing (fig. 12d). The hyperbolic-parabolic achieves a state of lower potential energy at the instability, while the total strain energy keeps increasing. The result is a more gradual negative stiffness at the instability.

Concluding, the transition of energy from the sides to the middle happens more gradual for the hyperbolic-parabolic. Since a considerable amount of the energy is already released at the sides before the instability, less energy can be released during the instability. Therefore, the balance between the energy release and increase during the instability remains positive yet becomes decreasing for the hyperbolic-parabolic. The cross section deforms more gradual and the strain energy and stress at the middle increase more gradual. The result is a more gradual negative stiffness over a longer range of rotation.

4 Experiment

4.1 Physical model

The physical model is 3D printed out of Polyamide 12 (PA 12) using Multi Jet Fusion (MJF). MJF is a powder based technology whereby a fusing agent and a detailing agent are jetted to selectively melt the powder particles. A great benefit of MJF is the use of fine-grained PA 12 material which leads to parts with low porosity and high density due to the thin layers of 80 microns. The result is a homogeneous shell, which is beneficiary to a more isotropic stress behavior in the shell.

To obtain the necessary rigid boundary conditions at the shell, solid blocks of PA 12 with a thickness of 2 cm are printed at the ends.

4.2 Measurement setup

For approaching a pure rotation and bending moment and lower the influence of reaction forces an aluminium hollow tube of 0.5m is attached to one end of the shell. The other end of the shell is clamped to a beam which is clamped to the table. For accurate measuring it is of high importance deformation occurs only in the shell and not in the setup used for the clamping. For this rigid attachment four clamps were used to attach the beam to the table. In fig13 the setup can be seen.

(a) Side view of the setup

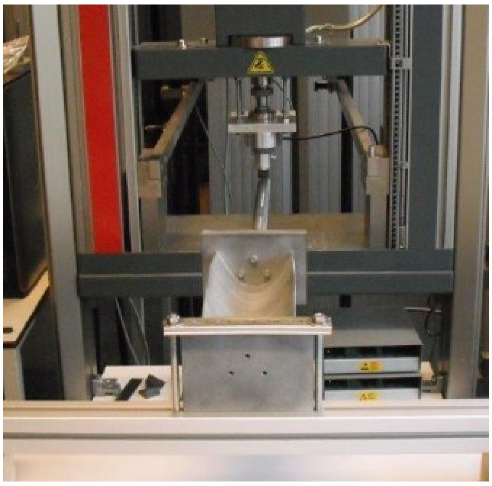

(b) More detailed picture of the clamping

Figure 13: Pictures of the measurement setup

A displacement is applied to the end of the aluminium tube by the tip of the machine and the needed force is measured by a load-cell. To make sure the machine touches the tube at the start of the displacement a pre-load of 0.1N is set. The flattening of the cross-section is determined by measuring the width of the shell with a caliper at the half of its length at the maximum of every displacement. To make sure the measurement is done accurately, the shell is kept at its maximum prescribed vertical displacement for 30 seconds at each time.

Since the shell will probably reach the limits of the stress that it can endure before breaking, it is tested by increasing the vertical displacement with a small step of 5mm each time. This way more data

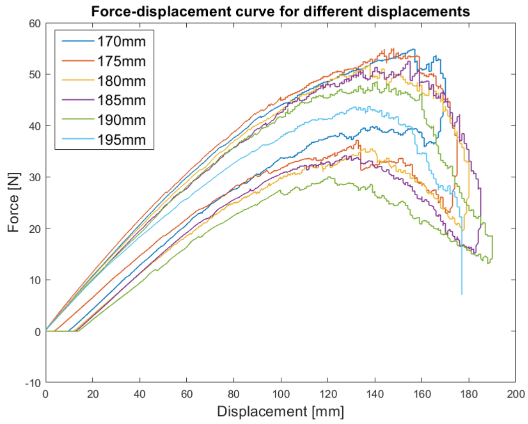

Figure 14: Measurement results. The force-displacement curves for vertical displacements of the tube end of 170mm until 195mm with 5mm steps. It is clear that the force needed for the displacement is decreasing around a vertical displacement of 150mm.

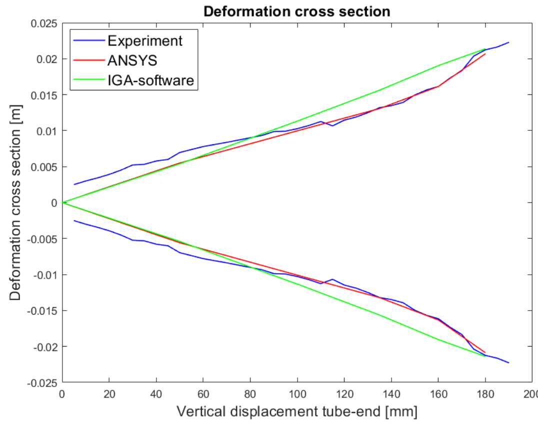

Figure 15: The deformation of the cross section in the experiment, ANSYS model and IGA model.

is achieved if it would break. To achieve quasi-static behavior the vertical downward displacement is applied at a rate of 20mm per minute. The vertical upward displacement, to return the shell to its initial position, is at a rate of 50mm per minute.

4.3 Results

In fig. 14 the results are shown for the applied vertical displacements of 170mm until 195mm. The force is measured by the load-cell for the vertical downward displacement. The shell is kept in its maximum prescribed position for 30 seconds. After that the force is measured when the shell returns to its initial position. When a vertical displacement of 195mm was set, the shell teared due to sudden torsion.

The force is at a maximum for each measurement at a vertical displacement of around 150mm, thereafter the measured force decreases.

The change in length of the end of the shell to the table was measured several times. By doing trigonometric calculations an assumption is made on the angle of rotation α of the shell during the vertical displacement. This is used for comparing the experimental data to the computer models.

The change in the cross section is measured over the whole width of the shell. In the computer models the displacement of the points $S1$ and $S2$ were used to measure the deformation of the cross section. Therefore the total width of the shell measured during the experiment is subtracted from its initial width. It is assumed that the deformation is the same for both sides of the shell and therefore the deformation is divided into two directions. A comparison of the deformation of the cross section is made between the ANSYS model, the IGA model and the experiment and is shown in fig. 15. The blue line indicates the deformation in the experiment, the red line in the ANSYS model and the green line in the IGA software.

5 Discussion

In this section different aspects of the research are discussed. First the general contribution, after that the computer models and at last the prototype and measurement results are discussed.

5.1 General contribution

The elongation of the range of negative stiffness during the rotation of tape springs is the main contribution of this paper. The negative stiffness can be used for static balancing over a rotational range of motion, which is a new application for the elastic instability in compliant shell mechanisms. The analysis shows that the addition of longitudinal curvature changes the stress and energy distribution in the shell before the instability. The transition of energy from the sides to the middle occurs for the tape spring mainly during the instability. For the hyperbolic-parabolic the transition develops mostly before the instability due to the added longitudinal curvature. The increasing deformation of the cross section before the instability contributes to this transition.

The way the shell is analyzed can be used to elongate the range of negative stiffness in other compliant shell mechanisms. The transition of energy and the deformation before and during the instability must be analyzed. The stress distribution can be predicted for changes in the geometry. A prediction can be made if the changes in the geometry encourage the deformation and energy transition before the instability. The result will be a more gradual change in potential energy during the instability, which results in a more gradual negative stiffness over a longer range of motion.

5.2 Analysis computer model

At first the models of the shells were built in the IGA software of Delft University of Technology. The advantage of this software is that it is relatively easy to create a moment-rotation curve, which made it simple to derive the stiffness behavior of the shell during the rotation α. A disadvantage is that it is difficult to determine the stress and energy behavior during the rotation for different areas of the shell. Therefore, models were made in ANSYS. In ANSYS the stress and energy analysis during the rotation was done, however, a moment-rotation curve for the behavior after the instability could not be made. By doing a strain energy analysis the negative stiffness behavior in the shell is indicated. For both models it is therefore shown that qualitatively the range of the negative stiffness is elongated.

Due to the differences between the software it is complicated to make a comparison between the two models, although some aspects can be compared. Quantitatively there is a clear difference in the angle of rotation α wherefore the instability in the hyperbolic-parabolic occurs. In ANSYS the instability occurs at $14°$ rotation, while in the IGA software at $11°$.

The deformation of the cross section is compared in fig. 15. From a quantitative perspective the shell in the IGA model has more flattening per degree of rotation α. A possible reason is the fact that the instability in the IGA model occurs for a lower rotation. Qualitatively it can be stated that both models have a gradual flattening of the cross section.

5.3 Experimental results

Since the nylon prototype is 3D printed the influence of the layers on the stress and strain behavior has to be taken into consideration. The production of a second prototype can point out the differences. However, the homogeneity and density of the prototype seemed high due to the thin layers of 80 microns and the influence of the layers seems to be minimized.

For approaching a pure applied rotation a simple measurement setup was build. A long moment arm is obtained by attaching a hollow tube at one end of the shell and applying the force at the end of the tube. The shell was attached with multiple screws to a steel bar and the bar was attached to the table by four clamps. More clamps were used than seemed necessary to minimalize the effect of the stiffness of the setup on the measurement.

The tip applying the force to the tube had solely a vertical displacement and started sliding over the tube due to the bending of the shell. This displacement resulted in an increase in the moment arm which influenced the magnitude of the moment on the shell.

Due to the sliding of the tip material was scraped off the tube. Since at higher forces more material was scraped off, more noise is seen in fig. 14 if the force increases.

The influence of the stiffness of the setup and the sliding of the tip over the tube make a quantitative comparison of the applied loads between the model and the experiment inaccurate. Qualitatively it can be seen from fig. 14 that the stiffness of the shell is decreasing until zero and after that becomes negative. The negative stiffness is observed in multiple measurements. It is not abrupt, as expected for a straight tape spring, but occurs gradually, resulting in a negative stiffness for a longer range of motion.

The applied force for the loading of the shell differs from the force during the unloading as can be seen in fig. 14. The reason for this is probably the stress relaxation that occurs in the shell. The stress decreases over time under a constant strain. The shell stayed at its set maximum for 30 seconds to make time for the measurement of the cross section. Therefore the material in the shell has a decreased tendency to return to its original shape when unloaded. For static balancing the change in applied force during the unloading is problematic and has to be minimized.

6 Conclusion

The objective of this paper was to obtain a longer range of negative stiffness in a compliant shell mechanism. For the first time it is shown that for a rotational range of motion the range of negative stiffness in compliant shell mechanisms can be elongated. The short and sudden negative stiffness during the snap-through behavior of a tape spring was used as a start.

For the tape spring and hyperbolic-parabolic the changes in terms of the deformation of the cross section, stress distribution and energy distribution before the instability are analyzed. The cross sections of both shells flatten since a state of lower strain energy is achieved. The influence of the flattening of the cross section on the stress density and energy distribution is determined. During the instability there is considerable change in the distribution of the stress and strain energy over the shells. Strain energy is released at the sides and arises at the middle. For the tape spring this results in a decrease in total strain energy. For the hyperbolic-parabolic the gradient of the energy becomes decreasing while the total strain energy keeps increasing.

It is shown that the addition of longitudinal curvature changes the stress distribution in the shell. This causes the majority of the transition of the energy to happen before the instability. The result is a more gradual transition of the energy during the instability, since less energy can be released at the sides. The cross section deforms more gradually during the instability and a more gradual negative stiffness is obtained.

The more gradual release of energy at the sides during the rotation results in a more gradual negative stiffness over a longer range of motion for the hyperbolic-parabolic compared to the tape spring. For validation of the model the stiffness behavior is tested during an experiment. A model was 3D printed and its stiffness behavior was investigated. The results show that during the rotation of the shell the stiffness decreases to zero and becomes negative afterwards The negative stiffness occurs gradual and over a longer range. The experiment qualitatively validates the model.

References

[1] van de Sande WJ Herder JL. Leemans JR, Kim CJ. Unified stiffness characterization of nonlinear compliant shell mechanisms. *ASME. J. Mechanisms Robotics*, 2018.

[2] G. Radaelli and J.L. Herder. Gravity balanced compliant shell mechanisms. *International Journal of Solids and Structures*, 118-119:78–88, jul 2017.

[3] Radaelli G. Kim C.J. Herder J.L. Nijssen, J.P.A. Overview and kinematic characterization of compliant shell mechanism building blocks.

[4] Nan Hu and Rigoberto Burgueño. Buckling-induced smart applications: recent advances and trends. *Smart Materials and Structures*, 24(6):063001, may 2015.

[5] Karin Hoetmer, Geoffrey Woo, Charles Kim, and Just Herder. Negative stiffness building blocks for

statically balanced compliant mechanisms: Design and testing. *Journal of Mechanisms and Robotics*, 2(4):041007, 2010.

[6] K. A. Seffen. On the behavior of folded tape-springs. *Journal of Applied Mechanics*, 2001.

[7] S. Pellegrino K.A. Seffen, Z. You. Folding and deployment of curved tape springs. *International Journal of Mechanical Sciences*, 42:2055–2073, 2000.

[8] L.G. Brazier. On the flexure and of thin cylindrical shells and other "thin" sections. *Proceedings of the Royal Society of London. Series A, Containing Papers of a Mathematical and Physical Character.*, 116(773), 1927.

[9] L.S. Srinath. *Advanced Mechanics of Solids*. Tata McGraw-Hill Publishing Company Limited, third edition, 2009.

4 Further recommendations

Negative stiffness over a longer range of motion is obtained by adding longitudinal curvature to the tape spring. The analysis was only done for the tape spring and the hyperbolic-parabolic. Other shells with instabilities during bending have to be investigated to broaden the design space. A promising type of shell mechanism is the curved-corrugated shell. A brief elaboration of the negative stiffness behavior in those type of shells during their structural instability is given in Appendix B. New insights in those shells will provide the possibility to develop more general design rules.

For stroke rehabilitation it is useful if the percentage of the gravity that is balanced can be tuned. The negative stiffness behavior has to be made tune-able to achieve this. Further research has to be done in the optimizing of the shape to the desired negative stiffness profile. Tailor-made devices can be designed for stroke rehabilitation patients by optimizing the shape.

One of the main challenges remains the attachment of the shell to the patient. The attachment has to be fixed-fixed and resulting forces on the shoulder have to be minimized. For making a useful prototype the attachment has to be further investigated. Thereby it has to be kept in mind that the device should be wearable.

Another challenge that remains is the needed constant force for a constant moment around the shoulder that was stated in chapter 2. Part of this force will be applied by the patient, since stroke patients often have some strength left in their arm. The other part of the force can be for example initiated by a second compliant shell mechanism. If the force of this second shell is not exactly constant, it is a possibility to tune the negative stiffness of the first shell.

Before a working prototype will be manufactured many challenges lay ahead. However, the negative stiffness over a longer range of motion is a first step towards a stroke rehabilitation device designed with a compliant shell mechanism.

5
Conclusion

The objective of the thesis was to design a stroke rehabilitation device for the upper-extremity with a compliant shell mechanism.

The thesis started with an introduction wherein the shortcomings of current stroke rehabilitation devices were briefly described. The advantages of a compliant shell mechanism to fill up this gap were stated.

In the second chapter it was shown that the upper-arm can be modelled as a hanging pendulum. For static balancing the shell must be able to balance the gravity of the arm over a certain range of motion. It was chosen to start with the balancing of the upper-arm when the arm is lifted and neglect the influence of the lower-arm on this movement. The need of negative stiffness for the static balancing was described.

The third chapter was the key contribution of this thesis. It is shown that the range of rotational negative stiffness in compliant shell mechanisms can be elongated. The short and sudden negative stiffness during the snap-through behavior of a tape-spring was used as a start. It is shown that the addition of longitudinal curvature changes the stress distribution in the shell. The deformation of the cross section and strain energy density in the shell before the instability changes due to the addition of the longitudinal curvature. The result is a more gradual change in deformation and transition of energy during the instability. This lead to a more gradual negative stiffness behavior over a longer range of motion for the hyperbolic-parabolic. The behavior during the instability was validated by an experiment.

A

Stroke rehabilitation therapy

Introduction

In 2018 in the United States 795.000 people experienced a stroke, this means one person every 40 seconds. Nearly 133.000 people were killed after having a stroke, which makes it ranked 5th among all causes of death in the USA. It also makes it the leading cause of serious long-term disability in the US [2]. Of all people that experience a stroke 80% has acute hemiparesis on the contralateral upper-limb and for over 40% this is chronically. This means they get a motor impairment at the upper-extremity. This impairment includes impaired motor control, muscle weakness and changes in muscle tone [1].

Treatment for stroke rehabilitation

For many stroke patients the ultimate goal of rehabilitation is to achieve a level of functional independence. They want to reintegrate into society and be able to perform activities of daily living (ADL) at an independent level.

Neuroplasticity: In the last decades neurological research has shown that the brain has the ability to reorganize itself. This means that the brain can be taught how to do certain movements again. In both healthy as injured brains this is a capacity. This reorganizing is called neuroplasticity. Studies have shown that neural changes in the brain are accompanied by motor recovery improvements for stroke patients [11].

Movement therapy: Movement therapy is based on neuroplasticity. By training the patients in doing certain movements the motor learning can be improved. The patient's motor learning improves because movement therapy leads to the sprouting of dendrites, formation of new synapses, alteration in existing synapse and the production of neurochemicals [1]. The recovery of those neural functions can be increased if the movements in the therapy meet the following demands:

- Repetitive
- Goal-directed (meaningful)
- Intensive

In [1] a simple example is given to describe those demands: *"if an individual tries to reach for a glass filled with water to attempt to drink (meaningful), 50 times (repetitive), thrice daily for four weeks (intensive). Motor improvement then achieved such as an increased range of elbow extension would be permanent in nature and could be applied in other task performances."* Thus, stroke rehabilitation methods should consist of intensive and repetitive practice of meaningful tasks.
By doing movement therapy motor recovery will improve. Herein there are two types of motor recovery: true motor recovery and compensatory motor recovery [1]. For true motor recovery the same muscles that were used during a movement before the injury are recovered. By alternative or undamaged pathways the commands from the brain are transported to the same muscles. For compensatory motor recovery alternative muscles are used by the patient to complete the task. The patient will be able to get certain tasks

done. However, true motor recovery is preferred because then the injured muscles are truly recovering, compared to healthy muscles being trained to do alternative tasks. An additional method than can be included is constraint-induced movement therapy (CIMT) [1]. The aim of this method is to enhance the use of the paretic arm by constraining the healthy arm. Stroke patients tend to use their healthy arm to do all their ADL, which reduces the motor recovery of the injured arm. By constraining the healthy arm the number of meaningful repetitions increases as well as the intensity of the movement.

Influence gravity balancing on movement performance Spasticity has a great contribution in motor impairments and limits stroke patients in their daily movements [9]. Patients experience an uncontrolled coupling between shoulder abduction and elbow flexion. When the arm is supported this coupling is less strong. An increased use of alternative pathways to compensate the damaged pathways probably results in the undesired coupling. This coupling is less strong when the arm is supported and the gravity is balanced.
Gravity balancing improves the ability of the patient to obtain true motor recovery in the upper-arm and shoulder. The activity of all muscles during reaching movements decrease when the gravity is compensated, however the general pattern stays the same. Meaning that all muscles are used in the same manor with and without gravity compensation. Muscles don't over- or under-compensate to execute the movement, meaning that the exercise contributes to obtain true motor recovery [8]
The muscle activity during movements is tested with and without gravity compensation. It was found that the muscle activity was lower during movements with gravity compensation [8]. The performance during the movement was comparable. Research indicates that gravity compensation has a positive influence on the movement performance. The active range of motion increases with gravity compensation.
The best treatment are movements that are used in ADL. Herein repetition is key to encourage the neuroplasticity of the brain. Neuroplasticity is the ability of the brain and other parts of the central nervous system to reorganize itself. This means that the brain can be taught how to do certain movements again. In both healthy as injured brains this is a capacity.
By balancing the gravity of the arm, the repetitive motion of the arm can be encouraged. Using the device at home would encourage the patient to practice more intensively. It is time consuming to visit a therapist every week and it can be difficult for patients to get there. Practicing at home will give them more time to practice. The device should be able to support certain movements used for ADL. This way the movements done by the patient for rehabilitation are task-specific and meaningful.

Current available arm rehabilitation devices for the arm

Different stroke rehabilitation devices for the arm are available. Different distinctions can be made. There are passive and active devices, wearable and unwearable devices and devices that have or have not to be used in a clinical environment. At first current available devices and their advantages and disadvantages will be elaborated in this section. After the missing gap in stroke rehabilitation devices is elaborated.

NeReBot (image in reference [7]): Three DC motors attached to nylon wires, which are attached to the arm, provide the movement of the arm. During the therapy the patient has to sit in a wheelchair or a bed. A clinician is needed to set up the robot and modify settings during the treatment. An advantage is that the robot-aided device guides the upper limb through a trajectory, which leads to improvement in motor and functional recovery. Besides, the degree of force that the patient has to apply can be modified. A disadvantage is that it is a robot that has to be used in a clinical environment. Therefore a therapist is needed and the patient is not able to do the exercises at home. This reduces the repeatability and intensity.

Freeball (image in reference [10]: This passive device uses two ideal spring mechanisms to balance the gravity of the arm. Both of the mechanisms are connected to the arm by cables, one at the wrist and the other at the elbow. The simplicity of the device makes it easy to use. Therefore it does not has to be used in a clinical environment, but can be used at home. Besides, the manufacturing of the whole construction is relatively simple compared to for example active robotic devices. However, it is a large construction, which needs a room with a high ceiling. If placed in for example in a living room, it takes a lot of space. This disadvantage makes it less convenient to use at home.

T-WREX (image in reference [5]: The device has a rigid body structure and uses elastic bands to compensate the gravity. The T-WREX is wearable and the gravity is well balanced. Studies show that an improvement in motor learning can be achieved. It is relatively simple to use compared to the active robotic devices. However, the disadvantage is that the assistance of a therapist is still necessary to use the device. The assistance is needed for the donning of the device. Also the range of motion (ROM) of the shoulder is limited because of the rigid body construction.

Missing gap For the upper extremity different types of devices are already established. As seen in fig. A.1 the grounded exoskeleton and the grounded end-effector are established. The next step is to develop a wearable exoskeleton [3]. A wearable device will improve the repeatability and intensity of the movement-therapy, which are key for stroke rehabilitation. Every day use of the device will be encouraged if it is wearable.

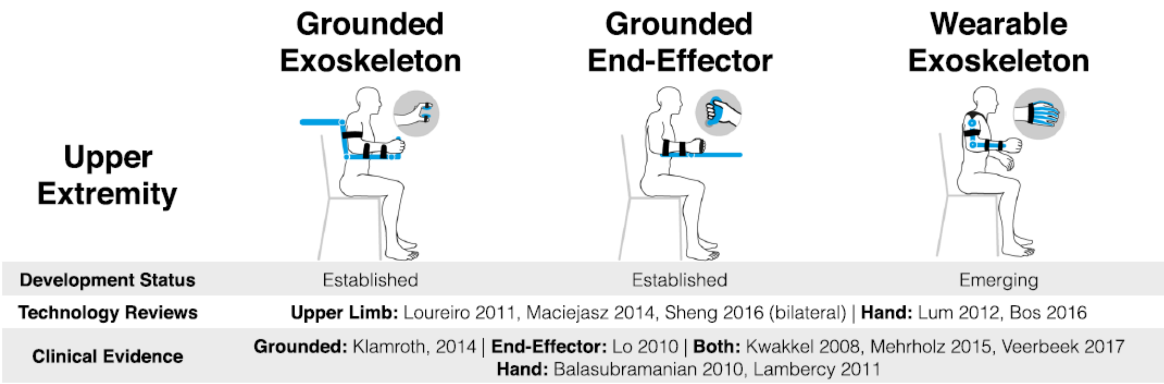

Figure A.1: Overview of the type of devices and their development status [3]

The active wearable devices that are currently available have the problem that they require large backpacks for the actuators. Besides, both passive and active wearable devices can only be used in a clinical environment or with the help of a therapist or expert. Therefore a device that is wearable and can be singly used by the patient at home is what is missing. The patient should be able to use the device without any assistance, the donning and doffing must be possible individually.

Benefit of a compliant shell mechanism A compliant shell mechanism can be made simple and easy to use. The shell can be produced with a relative light weight, which give patients the possibility for individual donning and doffing. The attachment can be complicated, but if done correctly the device can be made wearable.

Requirements needed for rehabilitation of the arm

As mentioned before, stroke patients lose their muscle strength after a stroke. Therefore everyday movements, like lifting their arm, are impossible or take too much effort to do. By balancing the gravity of the arm less strength is needed for the movements. Per patient it differs to what percentage the gravity has to be balanced and thereby does it change when patients make improvement. Therefore it is important that the percentage of balanced gravity is tune-able.

Research is done on healthy individuals to obtain the required range of motion (ROM) for certain ADL [4]. For the shoulder most ADL can be performed if the flexion and abduction/adduction of the arm can be done until the horizontal position of the arm. The horizontal abduction/adduction does not have to be gravity balanced. The sideways abduction/adduction and the flexion of the upper-arm need the same moment curve to be balanced, however the flexion of the elbow influences this movement differently.

It can be concluded that the upper-arm has to be balanced from a position vertical next to the body until the horizontal position. For stroke rehabilitation of the upper-arm the lower-arm has to maintain in the same position during the movement.

B

Curved-corrugated shells

Promising shells for creating tune-able negative stiffness in compliant shell mechanisms are curved-corrugated shells. For curved corrugated shells it is more difficult to predict the stress distribution and strain energy density in the shell. In this section the transition of the potential energy in the shell before and after the instability is shown. Thereby is the influence on the negative stiffness investigated. Since it was faster to create the shapes in the IGA-software instead of ANSYS, all analysis are done in this software. The shapes are created by the following equation:

$$x = Ay^2 - Ccos(\frac{n\pi z}{d}) + AB^2 \tag{B.1}$$

Wherein y is the width, which is $0.10m$ for all shapes and z is the height, which is 0.30 for all shapes. All shapes are rotated against the transverse curvature. Due to the corrugations there are "valleys" and "peaks" in the spine of the shell. Those references are used in the rest of this appendix.

B.1. Two corrugations

The following values are used in eq. B.1 to create the shell:
a=80 ; b=1 ; c=0.01 ; d=0.05 ; n=1
Below the moment-rotation curve is shown and the distribution of the potential energy for different rotations.

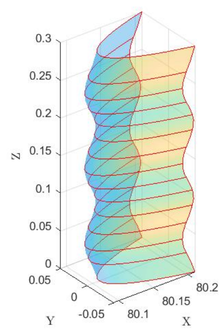

(a) Shell with 2 valleys and 3 peaks.

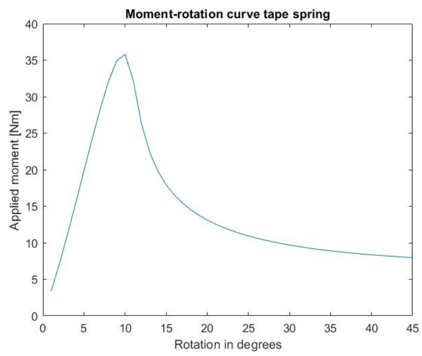

(b) Moment-rotation curve

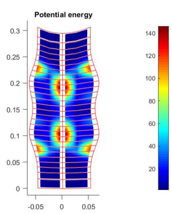

(c) 7 degrees rotation

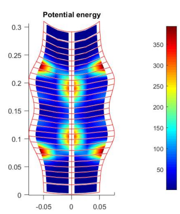

(d) 10 degrees rotation

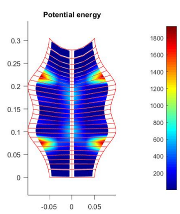

(e) 15 degrees rotation

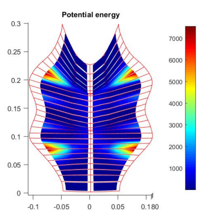

(f) 45 degrees rotation

It can be seen that there is a long range of negative stiffness. The potential energy is build up in the middle of the spine before the instability. During the instability there is a transition to the sides at the height of the folds. The folds are initiated around the two valleys of the shell.

B.2. More corrugations

More corrugations are added to the shape by changing n in eq. B.1.

n changed to 2: If more corrugations are added there is still a long range of negative stiffness (Fig. B.2). At first folds are formed more to the top and bottom of the shell. When further rotated folds arise more to the middle of the shell. From the moment-rotation curve it seems that there is a first and a second instability during the rotation. The energy starts again in the middle of the shell and there is a transition to the sides at the height of the first fold during the first instability. During the second instability there is a small transition of energy to the the sides at the height of the second fold.

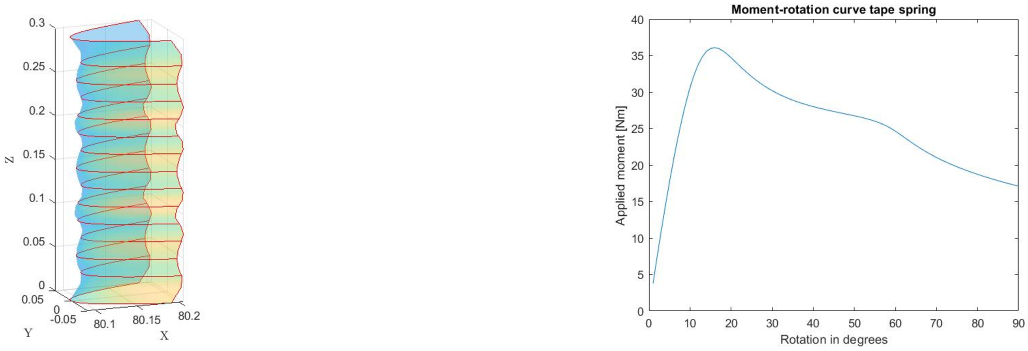

(a) Shell with 6 valleys and 5 peaks. (b) Moment-rotation curve

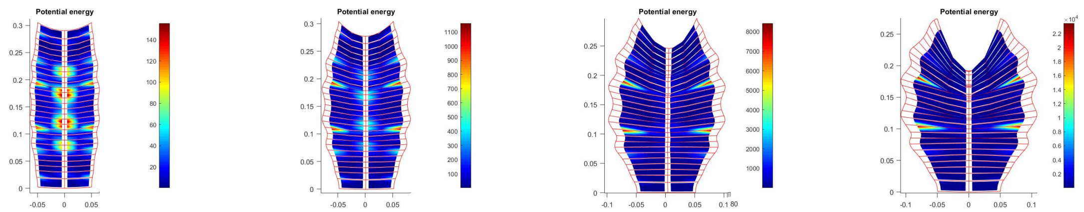

(c) 8 degrees rotation (d) 16 degrees rotation (e) 32 degrees rotation (f) 45 degrees rotation

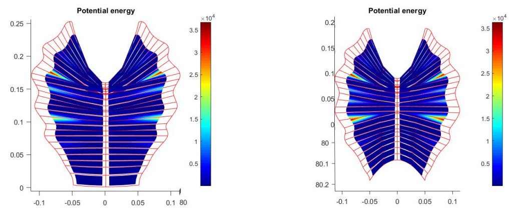

(g) 72 degrees rotation (h) 90 degrees rotation

Figure B.2: Shape for n=2

n changed to 3: Again it seems there are two instabilities (Fig. B.3). First there is a transition from the middle of the shell to the sides at the height of the first folds. During the second instability there is a transition to the sides at the height of the second folds, which are more to the middle. The main difference with the shell with $n = 2$ is the fact that this shell has a valley in the middle instead of a peak.

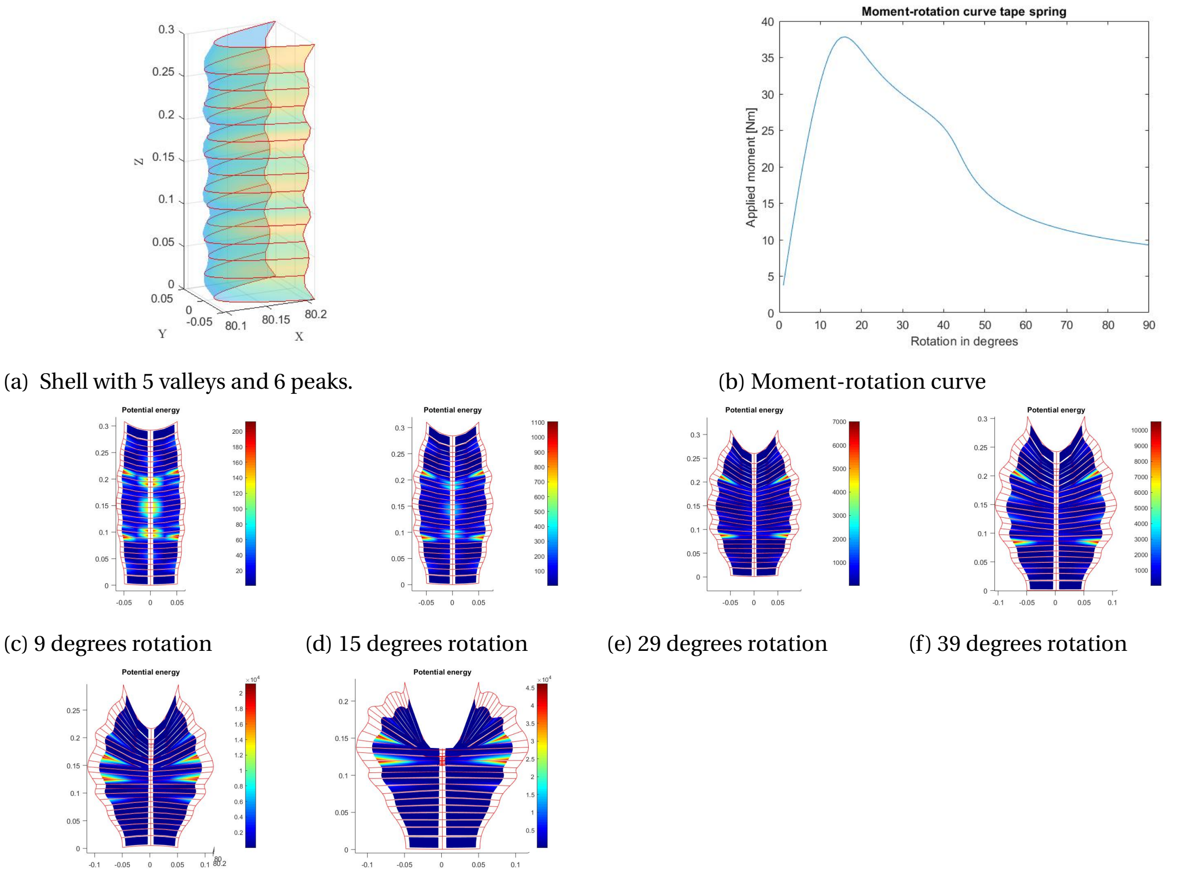

(a) Shell with 5 valleys and 6 peaks.

(b) Moment-rotation curve

(c) 9 degrees rotation

(d) 15 degrees rotation

(e) 29 degrees rotation

(f) 39 degrees rotation

(g) 55 degrees rotation

(h) 90 degrees rotation

Figure B.3: Shape for n=3

B.3. Two stages of instability

It is investigated what changes in the two stages of instability if the depth and/or length of the valleys are changed. The control points in the IGA software are changed to change the valleys. As a start the control points of the shell with $n = 3$ are taken. The control points can be seen in fig. B.6a, the moment curve is displayed again in fig.B.6b. It can be seen that at the left spine there are 5 valleys (corrugations) in total. The two on the outside and the one in the middle are longer and less deep. The two short ones between those are deeper. At the first stage of the instability the folds are at the short valleys, since the critical buckling load is lower compared to the middle valley. At the second stage the fold is at the longer middle valley. The applied moment has reached the critical buckling load of the middle valley.

There are again 5 valleys at the left spine (Fig. B.5). This time the four on the outside are longer and less deep. The middle one is shorter and deeper. Because the critical buckling load is this time lower for the middle, the only fold occurs around the middle. After this the stiffness is out of the middle of the shell and the outsides does not even buckle anymore. Therefore there is only one stage of the instability.

Again 5 valleys at the left spine (Fig. B.6. However, compared to the first simulation, the middle valley is now longer but with the same depth. The other 4 valleys are the same as the first simulation. In the moment graph it can be seen that there occur two stages of buckling. The first stage happens because of the buckling in the small valleys on the outside. After that the relatively long middle part flattens out until it buckles. Compared to the first simulation, this is way steeper buckling. This is probably because the cross-section of the flattened part that initiates the second buckling stage has a bigger area at this simulation

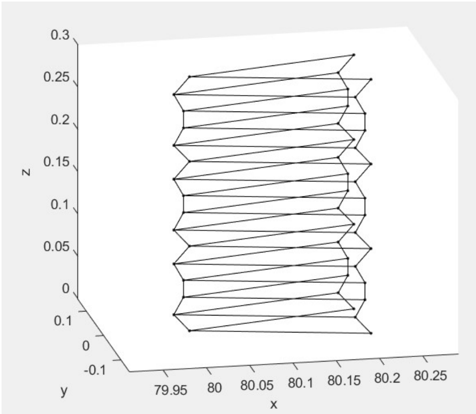

(a) Control points of the shell

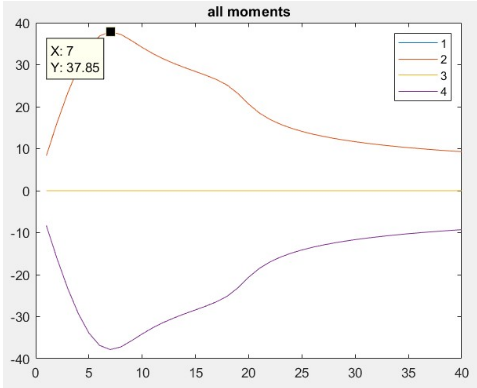

(b) Moment-rotation curve

Figure B.4: Shell with n=3

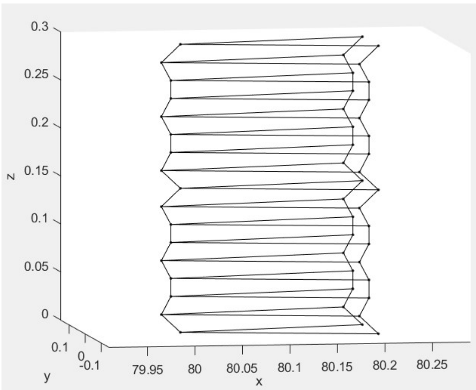

(a) Control points of the shell

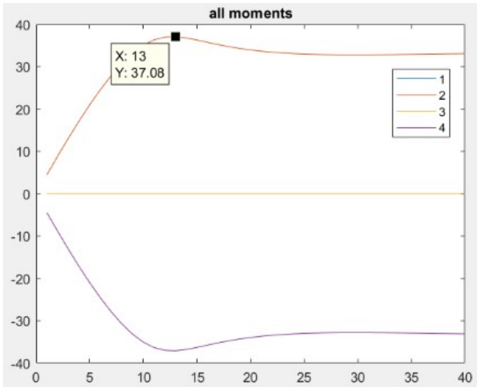

(b) Moment-rotation curve

Figure B.5: Shell with shorter middle valley

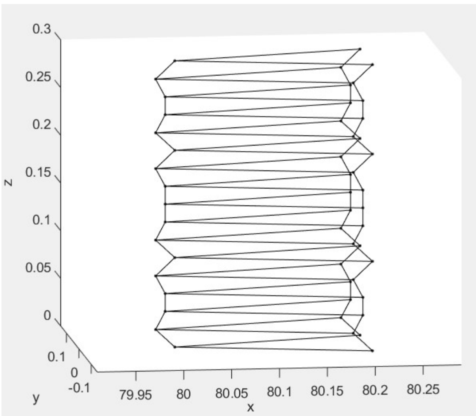

(a) Control points of the shell

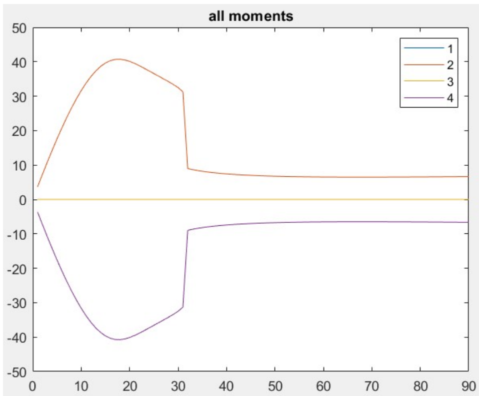

(b) Moment-rotation curve

Figure B.6: Shell with longer middle valley

A secondary buckling stage only occurs if the outsides of the shell buckles first because of a lower needed moment. If the middle of the shell buckles first, that is the only buckling that occurs. After that all the stiffness is out of the shell and no secondary buckling can occur.
The secondary buckling stage is initiated because the middle of the shell flattens out and loses stiffness. It seems that if the area of the flattened cross-section increases, the buckling becomes steeper. This can be seen

if the first and third simulation are compared. Because of the longer middle part at the third simulation the area of the flattened cross-section is bigger than at the first simulation.
It can be noted that the magnitude to initiate the buckling is for all shells shown above almost the same. This makes sense since the valley where the first buckling occurs at is for all shells the same length and depth. A pure moment is applied, which means the moment is for every cross-section the same in magnitude. So the buckling happens therefore first in those valleys.

B.4. Changing control points of the middle

The curved corrugated shell from fig. B.3a and fig. B.6a is build up out of three spines of 16 control points. The distance between the middle spine and the outside spines is always the same since the transverse curvature is constant. The y-coordinate is constant for every control point of the spine. The x-coordinates of the control points of the middle spine are the following:
$x_{middlespine}$ = [80.01 ; 79.9919 ; 80.0031 ; 80.0031 ; 79.9919 ; 80.01 ; 79.9919 ; 80.0031 ; 80.0031 ; 79.9919 ; 80.01 ; 79.9919 ; 80.0031 ; 80.0031 ; 79.9919 ; 80.01]
The first x-coordinate in the vector is at the height of the bottom of the shell. The following is at a constant higher height than its previous. The last is at the height of the top of the shell. The x-coordinates of the 8th and 9th control point are varied. This changes the depth of the middle valley of the curved corrugated shell. The x-coordinates of the middle control points are the following:
$Depthsmiddlecontrolpoints$: [80.0020 ; 80.0030 ; 80.0040 ; 80.0050 ; 80.0060 ; 80,0070]
It is investigated what the influence is if the middle valley (control points 8 and 9 of $x_{middlespine}$) are varied on the primary and secondary buckling stage. At first the valleys at the outside are deeper than at the middle for every x-coordinate of control point 8 and 9. After that the outside valleys are of almost similar depth as the middle valley.

B.4.1. Valleys deeper at outside than middle (80.010)

The x-coordinates for the outside valleys are at 80.010. Multiple runs are done wherein the top of the shell is rotated 45 degrees in 90 timesteps. The result can be seen in fig. B.7a. It can be seen that for the least deep middle valley the secondary buckling occurs more abrupt (data 1 in fig. B.7a). When the middle valley becomes deeper the secondary buckling stage occurs more and more gradual. At data 4, 5 and 6 there is a smooth transition between the primary and secondary buckling stage. A change in the depth of the middle valley has an influence on the first buckling stage as well. It happens almost at the same time, however for different applied moments. The maximum potential energy first occurs in the outside fold lines for the least deep valley (data1). At the secondary buckling stage there is a quick transition of the potential energy to the middle fold line. For the least deep middle valley (data 6) it seems that there is no primary or secondary buckling stage. However, from the potential energy behaviour it is seen that there is a first and second folding during the rotation. The transition of the max strain goes very slow and smooth from the fold lines on the outsides to the middle fold line. This results in the gradual negative stiffness.

B.4.2. Less deep outer valleys (80.0050)

This time the outside valleys are less deep than in the previous analysis. The top of the shell is again rotated 45 degrees in 90 timesteps. The x-coordinates of the middle two control points are again varied for the same values. It can be seen in fig. B.7b that there is no clear secondary buckling if the middle depth is just under or just above the outside valley depth. This can also be seen in the potential energy plot. The potential energy almost immediately occurs around the middle fold line after the negative stiffness occurs. There is barely energy at the outer fold lines. For clear secondary buckling it seems that the outer valleys should be way deeper than the middle valley.

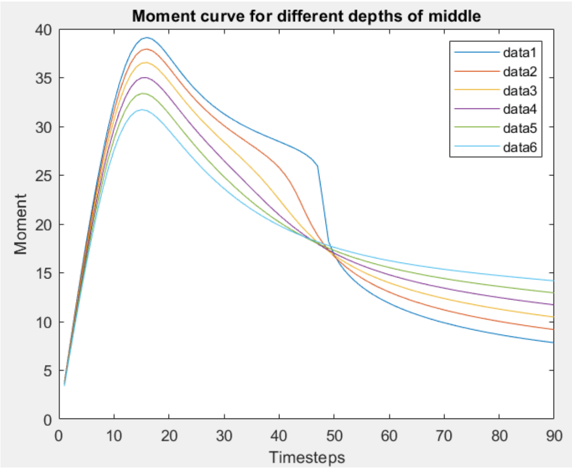

(a) Moment-rotation curve for changing depth of middle valley with x-coordinates for the outer valleys of 80.010. Data 1 is the least deep valley and data 6 is the deepest.

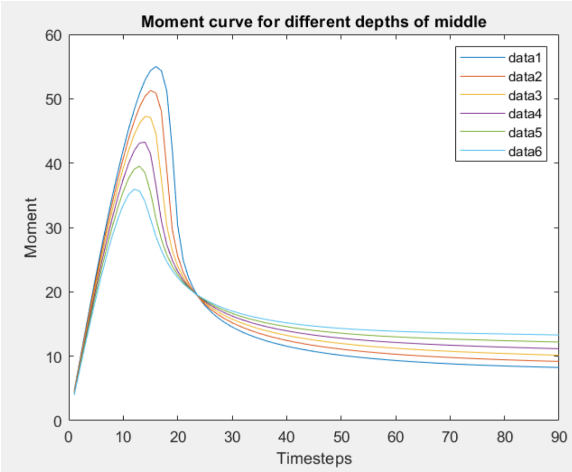

(b) Moment-rotation curve for changing depth of middle valley with x-coordinates for the outer valleys of 80.0050. Data 1 is the least deep valley and data 6 is the deepest.

Bibliography

[1] Kamal Narayan Arya, Shanta Pandian, Rajesh Verma, and R.K. Garg. Movement therapy induced neural reorganization and motor recovery in stroke: A review. *Journal of Bodywork and Movement Therapies*, 15(4):528–537, oct 2011. doi: 10.1016/j.jbmt.2011.01.023.

[2] Gert Kwakkel Boudewijn Kollen and Eline Lindeman. Functional recovery after stroke: A review of current developments in stroke rehabilitation research. In *Reviews on Recent Clinical Trials*, volume 1, pages 75–80, 2006.

[3] Roger Gassert and Volker Dietz. Rehabilitation robots for the treatment of sensorimotor deficits: a neurophysiological perspective. *Journal of NeuroEngineering and Rehabilitation*, 15(1), jun 2018. doi: 10.1186/s12984-018-0383-x.

[4] Deanna H. Gates, Lisa Smurr Walters, Jeffrey Cowley, Jason M. Wilken, and Linda Resnik. Range of motion requirements for upper-limb activities of daily living. *American Journal of Occupational Therapy*, 70(1):7001350010p1, dec 2015. doi: 10.5014/ajot.2016.015487.

[5] Sarah J. Housman, Vu Le, Tariq Rahman, Robert J. Sanchez, Jr, David J. Reinkensmeyer, Member, and IEEE. Arm-training with t-wrex after chronic stroke: Preliminary results of a randomized controlled trial. In *Proceedings of the 2007 IEEE 10th International Conference on Rehabilitation Robotics, June 12-15, Noordwijk, The Netherlands*. IEEE, 2007.

[6] Olga Kabel. One simple move to loosen up your shoulders. URL `http://sequencewiz.org/2016/03/16/loosen-up-your-shoulders`.

[7] Stefano Masiero, Andrea Celia, Giulio Rosati, and Mario Armani. Robotic-assisted rehabilitation of the upper limb after acute stroke. *Archives of Physical Medicine and Rehabilitation*, 88(2):142–149, feb 2007. doi: 10.1016/j.apmr.2006.10.032.

[8] G.B. Prange, M.J.A. Jannink, A.H.A. Stienen, H. van der Kooij, M.J. IJzerman, and H.J. Hermens. Influence of gravity compensation on muscle activation patterns during different temporal phases of arm movements of stroke patients. *Neurorehabilitation and Neural Repair*, 23(5):478–485, feb 2009. doi: 10.1177/1545968308328720.

[9] Disa K. Sommerfeld, Elsy U.-B. Eek, Anna-Karin Svensson, Lotta Wide
n Holmqvist, and Magnus H. von Arbin. Spasticity after stroke. *Stroke*, 35(1):134–139, jan 2004. doi: 10.1161/01.str.0000105386.05173.5e.

[10] Amo H.A. Stienen, Edsko E.G. Hekman, Frans C.T. Van, der Helm, Gerdienke B. Prange, Michiel J.A. Jannink, Arthur M.M. Aalsma, Herman Van, and der Kooij. Freebal: dedicated gravity compensation for the upper extremities. In *Proceedings of the 2007 IEEE 10th International Conference on Rehabilitation Robotics, June 12-15, Noordwijk, The Netherlands*. IEEE, 2007.

[11] D. David Ebaugh Surena Namdari, Gautam Yagnik. Defining functional shoulder range of motion for activities of daily living. *Journal of Shoulder and Elbow Surgery*, 2012.